Buried Empty Lava Tube Detection With GRAIL Data

Loic Chappaz,* Rohan Sood,† Henry Melosh,‡ and Kathleen Howell§
Purdue University, West Lafayette, Indiana, 47906, USA

The success of the NASA's GRAIL mission - a twin spacecraft formation revolving around the Moon in a quasi-circular polar orbit - currently provides the highest resolution and most accurate gravity data for the Moon. The low altitude at which some of these data were collected in the GRAIL extended mission potentially allows the detection of small-scale surface or subsurface features. This analysis is focused on the detection of the presence and extent of empty lava tubes beneath the mare surface.

I. Introduction

The twin Gravity Recovery and Interior Laboratory (GRAIL) spacecraft, named GRAIL-A and GRAIL-B, also known as Ebb and Flow, were launched in September 2011 as a Discovery-class NASA mission to study the gravitational field of the Moon.[1] After a cruise of several months, each spacecraft was inserted into their respective lunar orbit. Building on the success of the GRACE (Gravity Recovery and Climate Experiment) mission, a twin-satellite Earth orbiter mapping the gravity field of Earth since 2002,[2] extremely accurate range-rate measurements between the two spacecraft in the Ka-band wavelength (KBRR) enable the derivation of the Moon's gravity field with unprecedented resolution and accuracy. The GRAIL data were collected during two science phases, the nominal and extended mission. During the nominal mission, from March to May 2012, the spacecraft altitude was, on average, 55 km above the surface enabling the determination of an initial lunar gravity field model in terms of a spherical harmonic expansion up to degree and order 420.[3] Initiated in August 2012, additional data were collected until mid-December 2012 during the extended mission with a spacecraft altitude of 23 km on average, allowing the refinement of the gravity model to produce, currently, spherical harmonic solutions up to degree and order 900.[4,5] Also note that the data are recorded every 0.1 second, but are released at intervals of 2 or 5 seconds for an average altitude of approximately 55 or 23 km for the nominal and extended mission, respectively, while the spacecraft orbital velocities are approximately 1.25 km/sec. Also, the maximum offset between adjacent tracks is only at most a few fractions of a degree at the equator. The low altitude at which some of these data were collected in the GRAIL extended mission, with spacecraft altitude as low as a few kilometers over the lunar surface, potentially allows the detection of small-scale surface or subsurface features.

The focus of this investigation is the detection and extent of empty lava tubes beneath the mare surface. In addition to their importance for understanding the emplacement of the mare flood basalts, open lava tubes are of interest as possible habitation sites safe from cosmic radiation and micrometeorite impacts.[6] The possible or potential existence of such natural caverns is supported by Kaguya's recent discoveries of deep pits in the lunar mare.[7,8] Because the features of interest are beneath the lunar surface, traditional methods, such as surface imagery and altimetry, do not allow for the detection of such features. In contrast, since gravity is sensitive to both surface and subsurface features, gravity-like quantities can, in theory, be leveraged to probe the interior of the Moon. Thus, exploiting the gravity data collected by the GRAIL spacecraft, small buried features may be detectable. In this investigation, tools are developed to best exploit the rich gravity data toward the numerical detection of these small features. Two independent strategies are

*Ph.D Student, School of Aeronautics and Astronautics, Purdue University, 701 W Stadium Ave., West Lafayette, IN 47906; Member AAS, AIAA.
†Ph.D Student, School of Aeronautics and Astronautics, Purdue University, 701 W Stadium Ave., West Lafayette, IN 47906.
‡Distinguished Professor of Earth and Atmospheric Science, Purdue University, College of Science, 550 Stadium Mall Drive, West Lafayette, Indiana 47907-2051,
§Hsu Lo Distinguished Professor, School of Aeronautics and Astronautics, Purdue University, 701 W Stadium Ave., West Lafayette, IN 47906; Fellow AAS, AIAA.

considered: one based on gradiometry techniques, that is, a method that exploits gravity gradients, and a second that relies on cross-correlation of individual data tracks. Techniques that exploit gravity gradients are also employed on Earth to detect subsurface cavities,[9] changes in the crustal structure,[10] and even faulting events.[11] However, one key advantage to Earth-based analyses is the possibility for in-situ gravity surveys. For the lunar problem, both proposed strategies rely critically upon the unprecedented resolution and accuracy of the gravity data.

In this analysis, both detection approaches, that is, the gradiometry technique and the strategy that relies on cross-correlation, are combined into an automated algorithm that aims to construct local maps of the lunar surface and highlight the possible detection of features of interest. In addition, forward modeling is leveraged to further support possible detections and to attempt to characterize the physical parameters of a feature. The proposed algorithm is first validated using Schroeter Vallis, the largest known lunar sinuous rille, as a test feature. Then, another region near a South channel of Rima Sharp is introduced, where a persistent anomaly consistent with an underground mass deficit is identified. Finally, in an initial step toward inspecting the entire mare emplacements on the Moon, a global search strategy is introduced.

II. Lava Tube, Sinuous Rilles, and Skylights

II.A. Definition and Formation

Sinuous rilles have been extensively studied over the last several decades, starting with the Apollo missions, yet although a general formation mechanism is accepted, the details of the formation of such structures are not fully understood.[12] Sinuous rilles (SR) are usually characterized by sinuous channels of varying widths and depths with continuous walls. Often, these structures are associated with the presence of depressions of various morphologies that are interpreted as potential source vents for the lava flow that initially formed the channel. A rille typically terminates in a mare region, either abruptly as it intersects with a different mare unit, or by gradually fading into the mare. Most SRs are observed on the lunar near side in mare emplacements rather then on the far side or in the highlands. With the current understanding of the lunar environment and the surface geology, SRs are thought to be formed through lava flow and erosion processes, either in subsurface lava tubes that eventually collapsed or in surface lava channels. These features are numerous on the lunar surface and exhibit a wide variety in their morphology, including width, depth, length, and sinuosity. Although these features appear mostly in maria regions, the overall direction of the rille, if any, varies. In this analysis, the focus is directed toward the detection of potential empty subsurface channels, or lava tubes. However, because of the large number and the detailed information available for sinuous rilles, these structures represent relevant objects to test and validate the tools developed in this analysis. Also, SRs are most likely larger in dimension than potential lava tubes, hence, these features can be used to assess the limitations of the detection algorithm.

The formation of lava tubes is often associated with the formation mechanism of SRs. In essence, as an active lava flow, with sufficiently low viscosity, progresses along the lunar surface, a solid crust develops and thickens to form a roof due to radiating cooling driven by the high temperature gradient between the lava and the vaccuum. As the lava continues to flow in the now closed channel, it eventually leaves an empty subsurface tube with a hardened roof. Indication of the existence of such features is provided by the latest lunar missions. In particular, features labeled as 'skylights', that is, vertical holes that exhibit characteristics that cannot be explained as impact craters, are thought to be openings into empty subsurface lava tubes.[7,8] Such lava tubes are also found on Earth, although in much smaller sizes than the expected lunar features, as Earth gravity is much stronger. Sample structures of interest are illustrated in Figure 1 with characteristics provided in Table 1. In addition to the feature type and its location in the Moon-fixed Principal Axis (PA) frame in terms of longitude (λ) and latitude (ϕ), estimated dimensions are also given. The field 'main dimension' corresponds to the estimated length for a rille and the estimated diameter for a skylight.

II.B. Application to Human Exploration

Empty lava tubes are also interesting as possible habitation sites for human exploration endeavors, where the objective may be the establishment of a permanent base for lunar exploration or an outpost to support manned exploration beyond the Earth-Moon system. Such natural structures have been suggested as locations that are potentially safe from various hazards that are associated with the lunar environment, including

Table 1. Some features of interest

	type	λ, deg	ϕ, deg	main dimension	depth	width
Schroeter Vallis	Rille	301.7	24.5	175 km	534 m	4.27 km
Marius Hills Skylight	Skylight	303.230	14.091	$\simeq$ 50 m	$\simeq$ 50 m	N/A
Rima Sharp Channel	Rille	313.6	36.7	483 km	71 m	.84 km

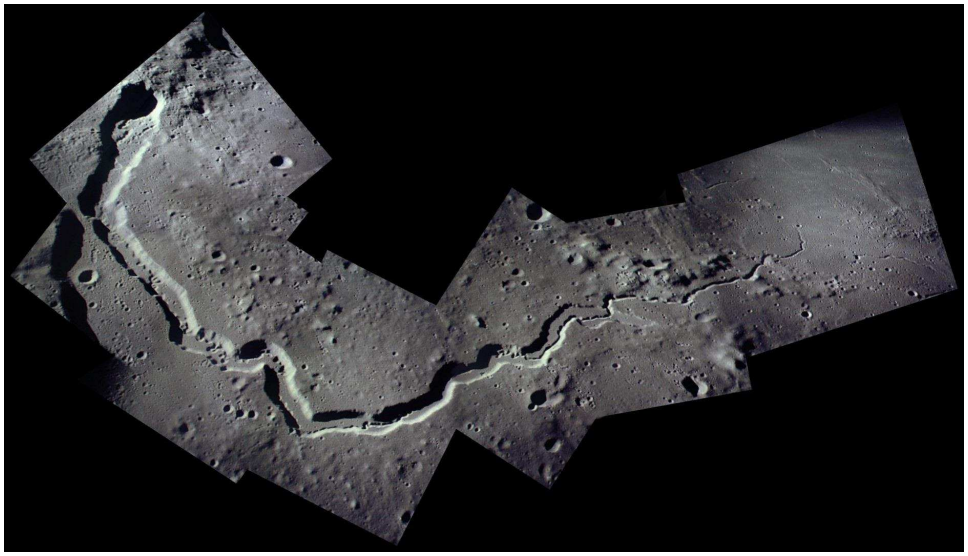

(a) Schroeter Vallis captured from orbit during Apollo 15 mission

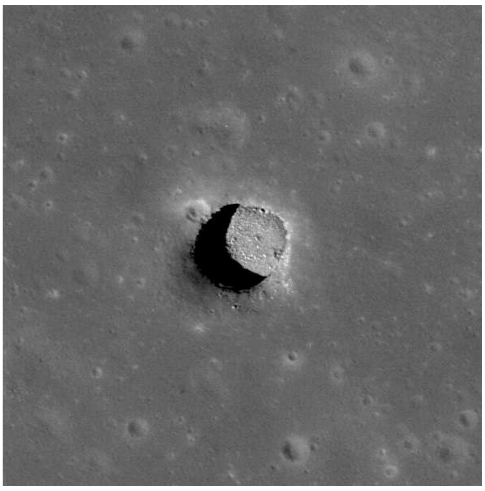

(b) Marius Hills pit near-nadir (0.5^o emission angle)image(M122584310L)

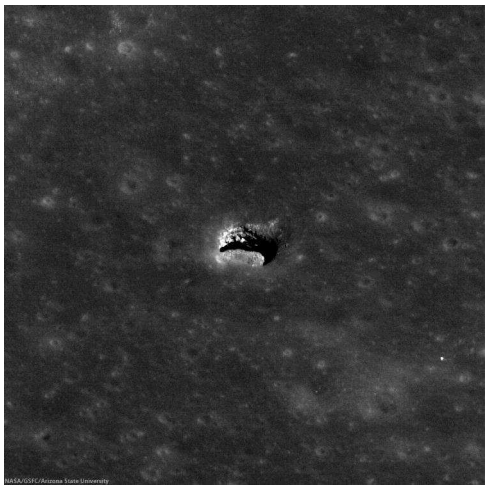

(c) M137929856R(34^o incidence angle and 45^o emission angle)

Figure 1. Schroeter Vallis and Marius Hills pit

cosmic radiation, micrometeorite impacts, and impact crater ejecta. Further, such sites would also provide a naturally regulated environment, with, in particular, a nearly constant temperature, in contrast to lunar surface conditions.[6] If such features exist in a preserved state, that is, empty channels - not collapsed - just beneath the lunar surface, these structure are not detectable through classical methods.

III. Detection Strategies and Validation Tools

III.A. Gravity Modeling

Extremely accurate range-rate measurements between the two GRAIL spacecraft in the Ka-band wavelength (KBRR) enable the derivation of the lunar gravity field with unprecedented resolution and accuracy. During the nominal mission, the spacecraft altitude was, on average, 55 km above the surface enabling the determination of an initial lunar gravity field model in terms of a Spherical Harmonic (SH) expansion up to degree and order 420.[3] Additional data were collected during the extended mission with a spacecraft altitude of 23 km, on average, that allowed the refinement of the gravity model to produce, currently, spherical harmonic solutions up to degree and order 900.[4,5]

III.A.1. Free-air and Bouguer potential and gravity

The gravity models produced from the data that are collected by the GRAIL spacecraft correspond to 'free-air' gravity, that is, the gravitational potential or force that is exerted by the Moon onto any particle of interest. In this analysis, the objective is to assess the existence of buried empty lava tubes. Within this context, 'Bouguer' gravity is also useful. Bouguer gravity is equivalent to the free-air gravity where the gravitational contribution from the surface topography has been subtracted, assuming topographical information is available. For the Moon, the topography is well-known given that one of the instruments onboard the Lunar Reconnaissance Orbiter (LRO), i.e., the Lunar Orbiter Laser Altimeter (LOLA), provides a precise global lunar topographic model.[13] Note that the 'standard', or crustal average, density assumed for the topography is derived from GRAIL data and assumed equal to 2560 kg/m^3. This value is probably not equal to the actual density of the lava; in samples the density ranges between approximately 3090 and 3170 kg/m^3[14] In essence, both surface and subsurface features can be observed in free-air gravity. Yet, some surface features may mask dimmer underground gravity anomalies. Assuming that the topography for a region of interest is well-known, Bouguer gravity only represents subsurface gravitational features and such a product may be more suited than direct free-air gravity, depending on the objective.

III.A.2. Truncation and taper

The SH model contains gravity information across the entire spectrum of frequencies, or wavelengths: from the lowest degrees that correspond to the tidal deformation of the Moon to the maximum degree of the expansion that depicts the subtle changes in density or topography of the Moon. To restrict the analysis to a domain that includes some features of interest, the SH expansion can be truncated on the low-end (low degree and order) to suppress the longer wavelength signals that correspond to the largest features (basins, tides,...) and on the high-end where the SH may not be representative of the actual data because of numerical artifacts. However, simple direct truncation of undesired degrees and order can result in a numerical challenge when evaluating the SH solution, an issue denoted as 'ringing'. To alleviate this effect, cosine tapers are applied where the field is truncated.

III.A.3. Gravitational potential and acceleration computation

The gravitational potential and the acceleration for the entire Moon are computed in this analysis using the high degree and order gravity models derived from GRAIL data. The evaluation of such SH series can be computationally expensive and also numerically challenging. Numerical errors in the computation of the Legendre polynomials for high degree and order computations generally cause concern. Thus, the spherical harmonic analyses are performed using the freely available software archive SHTOOLS (shtools.ipgp.fr) that is specifically developed to complete such tasks efficiently and accurately.

III.B. Gradiometry

The first strategy to investigate the existence of lava tubes relies on the numerical inspection of the lunar gravitational potential, computed from a set of spherical harmonics that is truncated and tapered to some predetermined degree and order to magnify the short wavelength structures of interest. From any scalar field, a widely employed method to detect or highlight ridges or valleys within the field of interest involves the computation of the Hessian, and consequently, the eigenvalues and eigenvectors that are associated with the Hessian of the scalar field. The Hessian of the gravitation potential is defined as the matrix of second partial derivatives of the potential function with respect to the spherical coordinates of the position vector, i.e.,

$$H_{ij} = \frac{\partial^2 U}{\partial x_i \partial x_j} \tag{1}$$

where $x_i, x_j = (\lambda, \phi, r)$, and r denotes the radial distance. In essence, the eigenvalue of largest magnitude and the corresponding eigenvector are associated with the direction of maximum gradient in the field. In this investigation, similar to the development in Andrews-Hanna et al.,[15] eigenvalue maps that depict the magnitude of the largest magnitude eigenvalue for each point on a grid of the lunar surface are produced. Either the free-air potential or the Bouguer potential (corrected for topography and terrain) can be employed in the analysis, depending on the objective. For the purpose of this investigation, localized maps that focus on specific regions are most relevant. Note that a sinuous rille or an empty lava tube corresponds to a negative gravity anomaly that reflects the relative mass deficit associated with the feature. Such a negative anomaly corresponds to a positive eigenvalue on the gradiometry map, or eigenvalue map, as a consequence of the additional derivative of the potential function in the computation of the Hessian.

III.C. Cross-Correlation

III.C.1. Method

A second strategy to explore the gravity data for evidence of lava tubes relies on directly exploiting the track data, that is, the relative acceleration of the two spacecraft as they move on their respective orbits. Only the horizontal component of the relative acceleration is directly available from the measurements, in contrast to the radial (i.e., vertical) or lateral components. In an initial effort to develop such a technique, proxy track data are created from available spherical harmonic models. The horizontal gravitational acceleration is computed along fictitious North-South tracks from the spherical harmonics. Then, track data are subdivided into individual tracks that correspond to a longitude value and a range of latitudes. Also, to exploit the assumed linearity of the lava tube, several tracks for a set of neighboring discrete longitudes are included within the same computation. The objective is then to identify the specific signature of a feature of interest within the generated track data. This task is accomplished by comparing the track data with a reference signal that represents the lava tube or sinuous rille through an analysis based on cross-correlations.

III.C.2. Reference signal

For a cross-correlation analysis, a reference signal, that is, a mathematical representation of the gravity anomaly due to the feature to be detected, is first constructed. Simple analytical expressions describe the acceleration anomaly experienced by a spacecraft along a flight path that is perpendicular to an infinitely long lava tube just beneath the surface; the tube is idealized as an empty horizontal cylinder. The horizontal acceleration component is calculated as,

$$g_{ref} = \frac{2Gm}{\sqrt{x^2 + h^2}} \sin\theta \tag{2}$$

where x is the along track distance from the feature, h is the spacecraft altitude, and $\theta = \arctan(x/h)$. Then, $m = \pi R^2 \rho$ is the mass deficit associated with the tube of radius R, ρ denotes the density of the surrounding terrain, assumed constant, and G is the gravitational constant. These relations are employed to construct a reference signal for the structures that are to be detected, that is, sinuous rilles or lava tubes. In Figure 2 is illustrated the horizontal acceleration sensed by the GRAIL spacecraft assuming an empty cylinder of diameter 1 km, given a flight altitude of 50 km (the average altitude for the nominal mission) as well as a distance of 20 km (the corresponding average altitude for the extended mission). Note the characteristic

shape of the signal with an amplitude of some fraction of a milligal, where 1 mgal equals $10^{-5} m/s^2$. The magnitude of this signal is well within the level of resolution and sensitivity supplied by the GRAIL data.

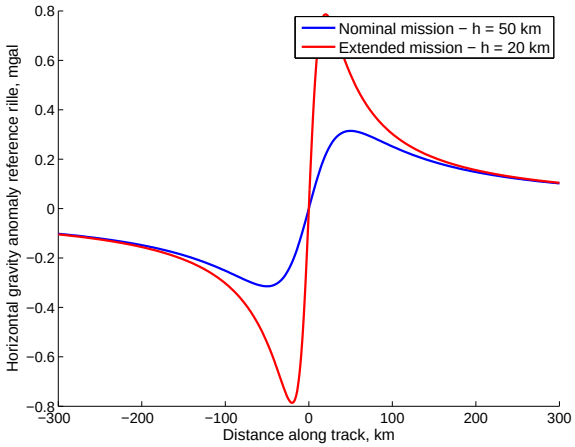

Figure 2. Analytical horizontal gravity anomaly.

III.C.3. Cross-correlation

Assuming a reference signal for the structures of interest is available, a mathematical construct is employed in the form of the cross-correlation between the reference signal and the spacecraft acceleration signal to assess the existence of such a feature within the data. In this implementation, the cross-correlation acts as a matching filter and the output of this comparison, the Cross-correlation Coefficient (CC), depicts the similarity of the reference signal relative to the track data. The cross-correlation also operates as a convolution operation, that is, the reference signal sweeps through the track, then, the CC assesses the similarity of the two profiles for each relative position of the two signals. Hence, a large positive cross-correlation coefficient indicates a location along that track where the spacecraft acceleration profile closely resembles the reference signal. Ideally, if a signature similar to the reference signal is present in the track data, a peak in the cross-correlation of amplitude larger than the background CC profile should be observed. However, recall that the reference signal used in this analysis is only an approximation of the actual gravity anomaly for a sinuous rille or a lava tube. The cross-correlation is defined as,

$$R_{xy}(m) = E\left\{x_{n+m} y_n^*\right\} = E\left\{x_n y_{n-m}^*\right\} \tag{3}$$

where $-\inf < n, m < \inf$, the operator E is the expected value, x and y refer to the track and reference signals, respectively. However, as the signal is, in fact, finite, the cross-correlation sequence is estimated as,

$$\hat{R}_{xy}(m) = \begin{cases} \sum_{n=0}^{N-m-1} x_{n+m} y^* & \text{if } m \geq 0, \\ \hat{R}_{xy}(m) = \hat{R}_{y^* x}(-m) & \text{if } m < 0, \end{cases} \tag{4}$$

where N is the larger number of elements between x and y, and $m = 1, 2..., 2N-1$. The CC is then defined as $CC = \hat{R}_{xy}(m-N)$ and is computed for any given track and scaled to values between -1 and 1. Also note that negative values of CC correspond to anti-correlation between the reference signal and track data, that is, the track data resemble the inverse of the reference signal.

III.C.4. Visualization

To address the challenge posed by the size of the features to be detected with respect to the gravity model resolution, the assumed linearity of shape of the lava tube is exploited. Several tracks from a set of neighboring but discrete longitudes are included in the same simulation. Then, rather than inspecting the raw CC for each individual track, the CC is employed as a scalar field and mapped onto the corresponding tracks to produce a two-dimensional cylindrical map, similar to the gradiometry approach. Since the cross-correlation analysis is performed on a set of discrete neighboring tracks, the CC computed for each track is used to interpolate a smooth CC field over the region covered by the tracks, labeled cross-correlation map.

III.D. Forward Modeling

The gradiometry and cross-correlation strategies rely on the gravity models derived from the GRAIL data to detect features of interest. It is useful to assess the validity of such detections. The concept that serves as a basis for the detection is a model that describes the gravitational signature of a feature and estimates the required parameters from the gradiometry or cross-correlation maps. Then, the gravitational potential and acceleration are computed for the forward model and incorporated into the simulation. The performance of the forward model is assessed by its ability to erase the observed signatures that should correspond to the feature of interest on the cross-correlation and gradiometry maps.

III.D.1. Point mass profile

A simple strategy models the gravitational signature of a mass deficit that corresponds to a sinuous rille or an empty buried lava tube by representing such a feature with a profile of discrete negative point masses. A 1-dimensional profile to mathematically construct the feature is a center line coupled with two additional lines of point masses to better represent the width of the feature. Such an approach is quite useful to model very sinuous structures. The total gravitational potential and acceleration due to the modeled features are then evaluated. The synthetic data are employed conjointly with the data produced from the lunar gravity models to assess the performance of the forward model.

III.D.2. Polyhedron shape model

Another strategy to represent the gravitational signature of a potential gravity deficit is a model that constructs the feature as a constant density polyhedron. There is no restriction on the geometric complexity in the polyhedron model and closed form expressions for the gravity potential, U, and acceleration, $\bar{\nabla}U$, are available, i.e.,[16,17,18]

$$U = \frac{1}{2}G\sigma \sum_{edges} \bar{r}_e \bullet \bar{\bar{E}}_e \bullet \bar{r}_e \cdot L_e - \frac{1}{2}G\sigma \sum_{faces} \bar{r}_f \bullet \bar{\bar{F}}_f \bullet \bar{r}_f \cdot \omega_f \tag{5}$$

$$\bar{\nabla}U = -\frac{1}{2}G\sigma \sum_{edges} \bar{\bar{E}}_e \bullet \bar{r}_e \cdot L_e + \frac{1}{2}G\sigma \sum_{faces} \bar{\bar{F}}_f \bullet \bar{r}_f \cdot \omega_f \tag{6}$$

where G is the gravitational constant, σ is the constant density of the structure, $\bar{r}_e$ and $\bar{r}_f$ are the vectors from the point field to the edge e and face f, respectively. Then, $\bar{\bar{E}}_e$ and $\bar{\bar{F}}_f$ are the edge and face dyads, respectively. The same procedure as described for the point mass approach is employed to assess the ability of the forward model to match a signature that potentially corresponds to the detection of a notable feature.

IV. Algorithm Development and Validation

IV.A. Algorithm

A strategy is introduced to detect small scale features on or beneath the lunar surface, an approach exploiting gravity information derived from GRAIL. Some level of confidence in the validity of the detection scheme is necessary, of course. The process is currently automated and conjointly exploits the gradiometry and cross-correlation strategies. Recall that for the first method, gradiometry, the gravitational potential is inspected through the eigenvalues of the Hessian of the potential function, while the cross-correlation technique relies on analysis of the horizontal gravitational acceleration.

IV.A.1. Challenges

The proposed strategy attempts to cope with some of the challenges associated with the detection of such small scale features. The predominant challenge in this analysis is the size of the features to be detected with respect to the spatial resolution of the spherical harmonics gravity model. Also, one consequence of evaluating the SH solution up to high degree and order, relative to the maximum degree and order of the field expansion, is numerical noise. Note that this numerical artifact does not correspond to noise in the measured data but is a product of the numerical methods involved in the representation of the data, that is,

the spherical harmonics expansion. Further, for the gradiometry approach, the computation of the Hessian of the potential function and the corresponding eigenvalues also relies on numerical schemes that are subject to numerical errors. Thus, signatures on a gradiometry map or a cross-correlation map may or may not correspond to a physical feature on the Moon. Specific measures are adopted to increase the robustness of the detection process.

IV.A.2. Computation

For a given gravity model, both free-air and Bouguer, the gravitational potential and the gravitational acceleration vector in spherical coordinates with respect to the Moon-fixed Principal Axis (PA) frame are computed using SHTOOLS for the entire Moon on a regular constant radius spherical grid. Additionally, the Hessian of the potential function and the eigenvalues that are associated with that functional are also computed. From this global computation, data that correspond to a region of interest are extracted to complete the cross-correlation analysis and produce cylindrical maps reflecting the largest eigenvalue and the cross-correlation coefficient. Recall that the Bouguer gravity is equivalent to the free-air gravity where the gravitational contribution from the surface topography has been subtracted. Thus, on a free-air map, both surface features, e.g., surface craters, sinuous rilles, and buried structures, such as buried craters or potential lava tubes, appear. In contrast, on a Bouguer map, assuming the topography is known to a spatial resolution that is equal or smaller to that of the features of interest, only underground structures appear. In other words, a buried lava tube should appear in both free air and Bouguer gravity, while an open rille, such as Schroeter, should be visible in free air but not in a Bouguer map, assuming that the density destitute for the surrounding topography is correct. Therefore, producing both free-air and Bouguer maps allows assessment of a potential feature as a surface expression or a buried structure. Further, to assist the identification process, a third map that depicts the correlation between the free-air and Bouguer map for a given model is also produced. In this analysis, the focus is the detection of empty buried lava tubes, that is, a mass deficit or, equivalently, a negative gravity anomaly. Such an anomaly is depicted by a positive eigenvalue for the gradiometry method and a positive cross-correlation coefficient for the second strategy. To further highlight a correlation between signatures that corresponds to a mass deficit, any correlation between the free-air and Bouguer maps that corresponds to a negative signal, i.e., a mass surplus, for either the eigenvalue or cross-correlation maps, is set to zero. Hence, positive signatures on the third correlation map depict locations where a signal consistent with the expression of a buried feature is observed.

IV.A.3. Visualization

To address the challenge posed by the size of the features to be detected with respect to the gravity model resolution, numerous individual simulations are leveraged. First, the initial gravity model is truncated and tapered to a range of degrees assumed to be reasonable and include the features of interest. Then, variations in the truncation on both ends of the field are employed to produce different SH solutions, yet all representative of the same data. The computation described in the previous section is performed for each modified gravity model to produce the corresponding maps. Finally, the results are inspected either through a static or dynamic representation. A map averaged over all simulations is produced as well as an animation of each individual map. While some signals may vary from one map to the next due to numerical artifacts, the average map supplies a cleaner representation of the region of interest. Similarly, the animation is insightful to emphasize signals that are persistent through the numerous simulations against signals that flicker and do not relate to physical features on the Moon.

IV.B. Application to Schroeter Vallis

For the purpose of this analysis, localized maps that focus on specific regions are most relevant. Consider a region in the Aristarchus plateau that contains Aristarchus crater and one of the largest known lunar rilles, Schroeter Vallis, as illustrated in the LOLA topography map in Figure 3. For this application, four gravity models are considered, two up to degree and order 900, one up to degree 720, and a final model up to degree 780. Then, as outlined in section IV.A.2, each model is truncated on both ends of the SH expansion and tapered to attenuate the resulting ringing. To increase the robustness of the simulation, various truncations for the low-end are explored, ranging from no truncation to eliminating the first 90 degrees and orders in the SH series. Further, each of the models already truncated at the low-end is also truncated at the opposite

end, that is, high degrees and orders are also eliminated. Similar to the low-end operation, several different truncations for the high-end truncations are applied. Thus, a multitude of modified gravity models are produced, all representative of the same initial data, but with various lower and upper truncations.

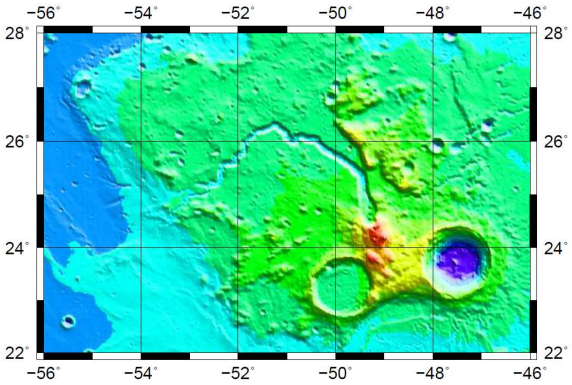

Figure 3. Local topography in the Schroeter Vallis region.

IV.B.1. Gradiometry

A simulation is performed for the localized region near Aristarchus plateau for the specified gravity models, Figure 4 illustrates the corresponding local averaged eigenvalue map for free-air and Bouguer potential, overlaid with the local topography from LOLA. The color scale represents the signed magnitude of the largest magnitude eigenvalue of the Hessian of the gravitational potential. From these local maps, it is now evident that the structure that emerges from the free-air map does, in fact, corresponds to the presence of the rille. Note that, as expected since the rille is a surface feature incorporated in the topography, there is no corresponding signal on the Bouguer map.

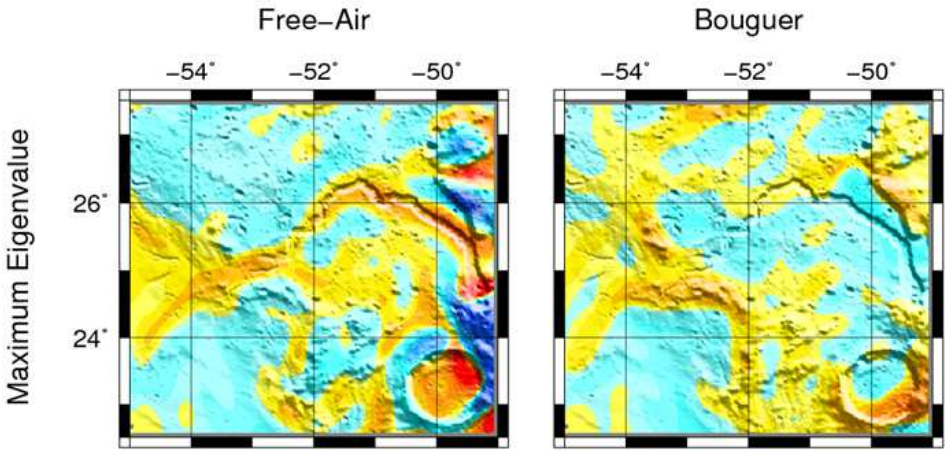

Figure 4. Local eigenvalues map in the Schroeter Vallis region with an overlay of topography.

IV.B.2. Cross-correlation

The second strategy in an attempt to detect buried lava tubes relies on leveraging the gravitational acceleration as modeled by GRAIL data and the expected acceleration anomaly a spacecraft would experience as it flies over a mass deficit. Figure 5 illustrates the cross-correlation map obtained from the simulation. This figure is constructed from the cross-correlation between 80 tracks of data and a reference signal constructed assuming a 2 km diameter lava tube and an altitude consistent with the spherical harmonic model (the spherical harmonic data are presented at the reference altitude whereas the track data must be evaluated at

the actual spacecraft altitude). The color scale represents the cross-correlation coefficient, from dark blue to red (a range from -1 to 1). The more positive the value of the coefficient, the more closely this portion of the track data resembles the reference signal, given that the cross-correlation operates as a matching filter. The rille signal corresponding to the topographic Schroeter Vallis clearly appears on the free-air cross-correlation map and is absent of the Bouguer map, consistent with the gradiometry results. This simulation offers a first validation of the scheme employed to detect the features of interest. These results also demonstrate the ability of the algorithm to produce clear maps of the eigenvalues and cross-correlation coefficient despite the numerical challenges that are associated with such computations.

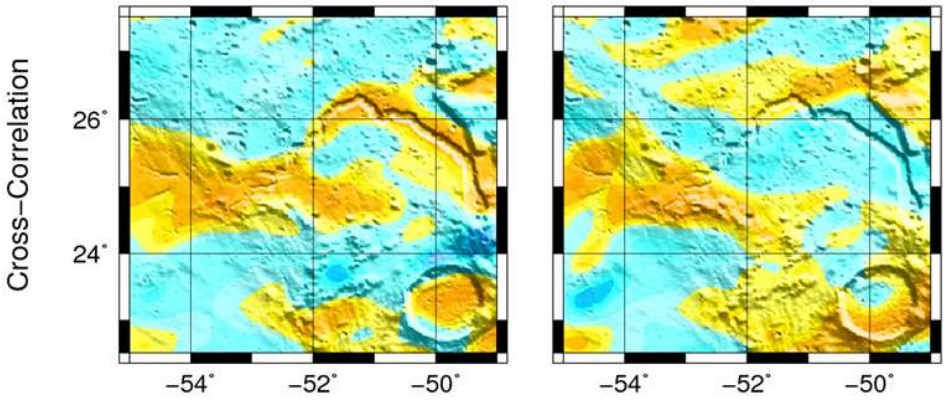

Figure 5. Local free-air (left) and Bouguer (right) cross-correlation map in the Schroeter Vallis region with overlay of topography.

IV.B.3. Forward modeling

In the Schroeter Vallis scenario, the structure that is detected is known and of a large size relative to other neighboring features. Nevertheless, forward modeling is applied to assess the usefulness of such a technique in the search for other small scale features whose detection may be more ambiguous. Schroeter Vallis is very long and sinuous, with a characteristic arch shape; thus, a point mass representation to construct the forward model appears more appropriate than a polyhedron model. First, a point mass distribution is defined to represent the feature. Two linear profiles comprised of point masses are used to give the model a shape and a third profile is computed as the center line, as illustrated in Figure 6(a). Then, the total mass deficit that corresponds to Schroeter Vallis is estimated using the simple trapezoid model that appears in Figure 6(b). The dimensions of the trapezoid, i.e., L, H, b_1, and b_2 are automatically determined from the point mass distribution exploiting LOLA topography. The same simulation to produce the averaged maps in Figures 4 and 5 with the gradiometry and cross-correlation methods, respectively, is repeated incorporating the gravitational potential and acceleration due to the forward model. The averaged maps for free-air gravity produced with this strategy are illustrated in Figure 7. Note that the gradiometry approach is more successful in matching the observed signal using the forward model; this discrepancy arises from the limitations that are inherent to the cross-correlation strategy. However, this simple test demonstrates the ability of a simple model to reproduce some of the observed signals that depict the anomaly associated with Schroeter Vallis. In the top right plot, the forward model that is incorporated in the simulation clearly erases the previous signature that corresponds to Schroeter Vallis, as observed in the left plot. Some limitations are associated with this analysis and are apparent in the Schroeter simulation. As mentioned, the predominant challenge in detecting these small scale features is the relative size with respect to the resolution of the gravity field. Also, there are some numerical difficulties that are associated with evaluating the SH series to very high degree and order. These challenges are successfully addressed by the proposed technique, to some extent. Another limitation, further specific to the cross-correlation procedure, is inherent to the strategy. In view of incorporating actual track data in the future analysis, the proxy track data generated from the spherical harmonics models are constructed in terms of discrete North-South tracks. Then, the simple reference signal that is used in the cross-correlation operation is derived assuming a spacecraft flies perpendicularly over an infinitely long tube. Therefore, the cross-correlation coefficient is more sensitive to features that are oriented East-West. Although the overall orientation of Schroeter Vallis may be described as East-West, the

sinuous channel also exhibits some arcs that are oriented nearly North-South, reducing the performance of the cross-correlation strategy for these regions.

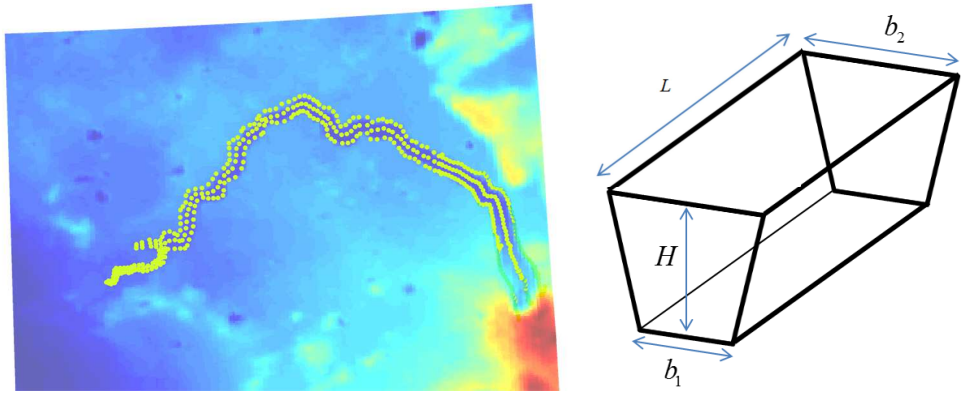

(a) Footprint (b) Shape model

Figure 6. Forward model for Schroeter Vallis

IV.C. Application to a Region without Known Features

The proposed algorithm successfully detects Schroeter Vallis, both with the gradiometry and cross-correlation strategies. However, because of the relative size of the features of interest compared to the resolution of the gravity field, combined with the numerical challenges that are associated with evaluating SH expansions at high degree and order, concerns regarding the validity of potential signatures that may be observed on the eigenvalue and cross-correlation maps naturally arise. Thus, another test is conducted that aims to demonstrate that a region with no known suface features triggers no detection when subjected to the same proposed analysis. Consider a small mare region southwest of the Aristarchus plateau region, as illustrated in Figure 8, no features of note within the context of detecting large sinuous rilles, are observed, in contrast to the Aristarchus region considered previously. For this region, a simulation sequence similar to the Schroeter region analysis is performed. Both the gradiometry and cross-correlation strategies are applied to a large number of gravity models to produce an averaged eigenvalue and cross-correlation map. In addition, given no a priori information regarding the existence of significant surface or subsurface features, a third map that depicts a bias correlation between free-air and Bouguer maps is also generated, as illustrated in Figure 9. As apparent on the gradiometry and cross-correlation maps, for free-air and Bouger gravity, no signature emerges from this simulation and this region does not appear to exhibit any significant surface or subsurface features that resemble a sinuous rille or lava tube. Further, the rightmost maps correspond to the correlation between free-air and Bouguer gravity, a strong correlation indicative of potential underground features would appear as a hot colored signature, however, no such signal is observed. This test achieves the simple purpose to validate that the averaging method successfully eliminates the numerical noise from the computation and produces a clear map that highlights physical significant features.

V. Detecting Underground Structures

Tools to detect small scale features on or under the lunar surface are developed and tested against the largest known lunar rille, Schroeter Vallis. The objective of this analysis is then to investigate the potential existence of intact empty lava tubes beneath the lunar surface.

V.A. Strategy

As features of interest, subsurface empty lava tubes, have no direct surface expression. Thus, regions around known surface rilles are initially examined to initiate the investigation. No systematic search strategy is exploited to yield the initial results, rather, the extensive data base of sinuous rilles compiled in Hurwitz et al.[12] is used to generate locations of interest. For the purpose of detecting such features with the tools developed in this analysis, that is, tools that rely on gravity information, the driving parameter for a detection

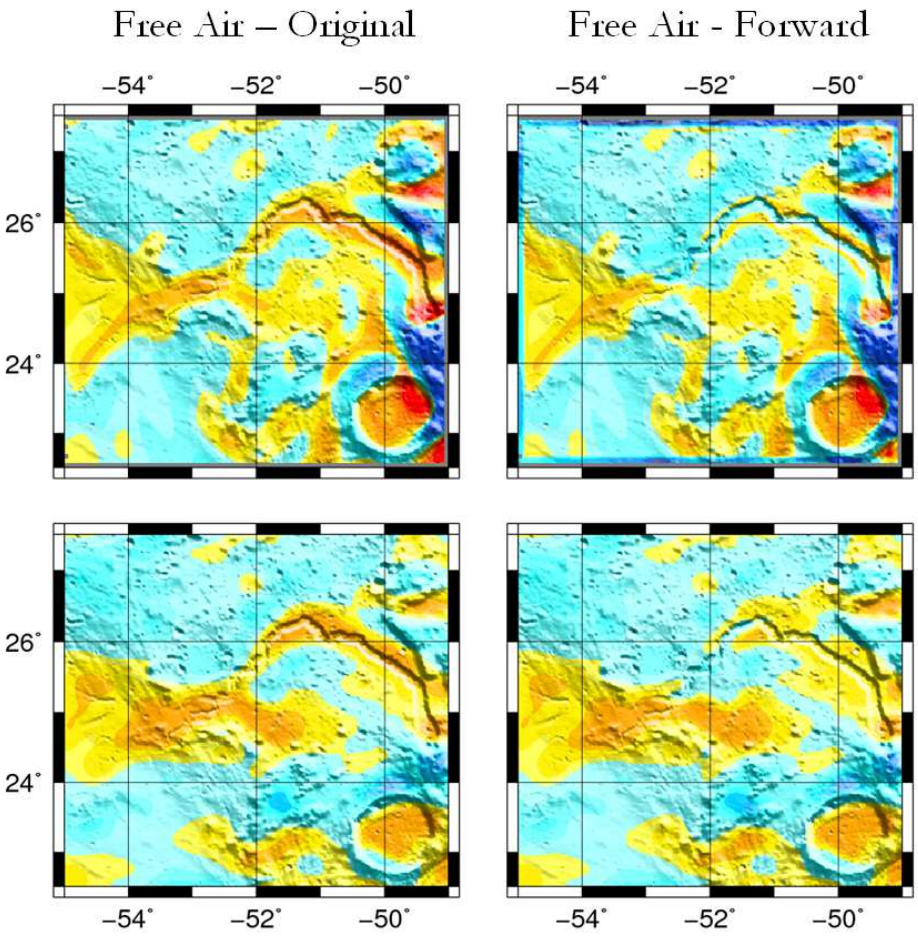

Figure 7. Local free-air gradiometry (up) cross-correlation (down) map in the Schroeter Vallis region without (left) and with (right) forward model.

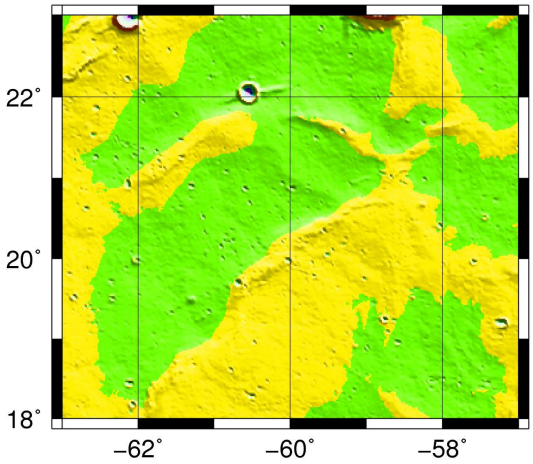

Figure 8. Local topography.

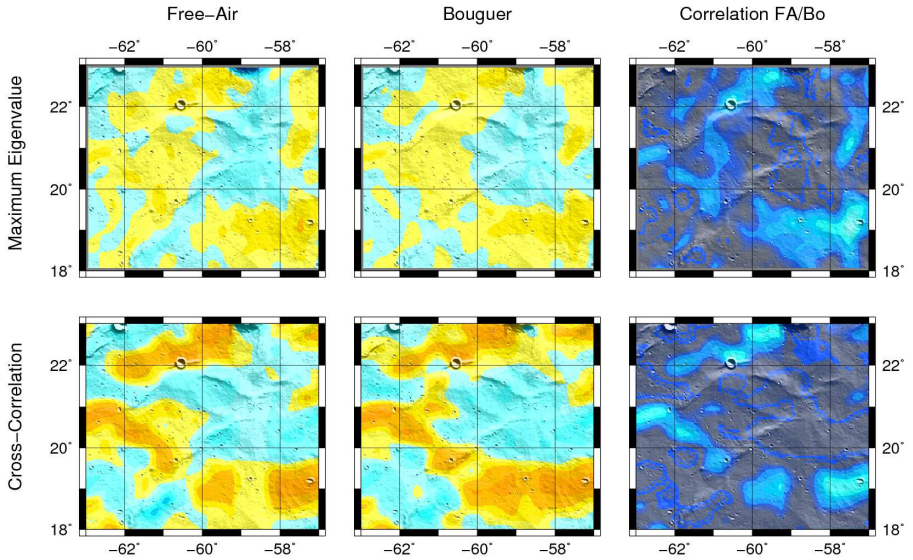

Figure 9. Local gradiometry (up) cross-correlation (down) map for free-air (left), Bouguer (center), and free-air/Bouguer correlation.

is the mass deficit that corresponds to the structure of interest. Thus, more emphasis is focused on deeper and wider rilles rather long ones. In addition, the spatial resolution of the gravity model compared to the size of these features is also a concern. Then, thin long rilles may appear more challenging to detect than short yet wider or deeper features.

V.B. Application to Rima Sharp

Besides Schroeter Vallis, Rima Sharp is an example of a large known sinuous rille. Initially, the objective for this scenario is to further test the ability of the algorithm to detect small scale features. An image captured by the Wide Angle Camera (WAC) aboard the LRO spacecraft appears in Figure 10, a notable feature runs from the top of the image toward the bottom, that is, a south channel of Rima Sharp is visible. This channel is, however, much smaller in size than Schroeter Vallis.

V.B.1. Gradiometry and cross-correlation simulation

Consider a region around a South channel of Rima Sharp, that is, for longitudes from 311^o to 316^o and latitudes from 35^o to 40^o. For this region, a simulation similar to the Schroeter region analysis is completed. Both the gradiometry and cross-correlation strategies are applied to a large number of gravity models to produce an averaged eigenvalue and cross-correlation map. In addition, as there is no a priori information regarding the existence of additional significant features underground, a third map that depicts a bias correlation between free-air and Bouguer maps is also generated, as illustrated in Figure 11. Although the Rima Sharp channel in the center of the figure is not resolved, another signal is observed along the bottom of the maps. This signal is present on the maps generated with both methods, gradiometry and cross-correlation, and on the free-air and Bouguer maps suggesting an underground feature. Also recall that these maps are the product of numerous simulations, a few hundred, and for a feature to appear on an averaged map it must be consistent through many individual computations. A less robust feature is eliminated from the map through the averaging process. Finally, the correlation map between the free-air and Bouguer gravity further highlights the observed signature. While few other signals that do not seem to correspond to surface features are observed on the gradiometry or cross-correlation maps, for free-air or Bouguer gravity, only the signature that corresponds to the identified potential underground feature is associated with a

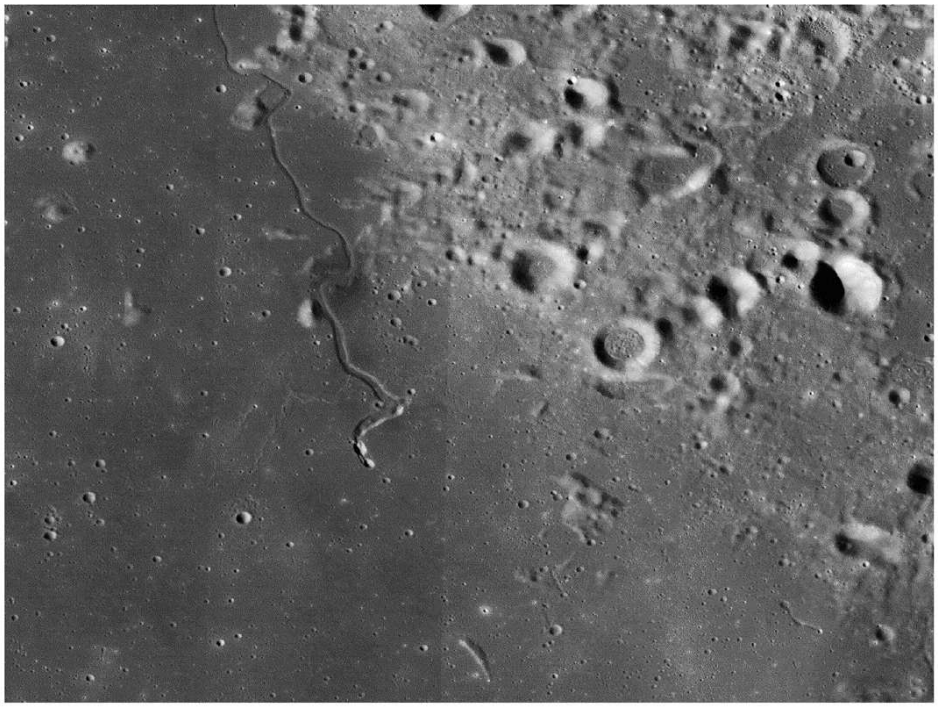

Figure 10. LROC WAC image near south channel of Rima Sharp.

strong free-air/Bouguer correlation for both strategies. All these observations strongly suggest the presence of an underground mass deficit that corresponds to a gravity anomaly.

V.B.2. Forward modeling

To further assess the validity of the signature observed on the gradiometry and cross-correlation maps, and in an initial attempt to physically characterize the feature that may cause such an anomaly, a forward model of the potential structure is developed. From the map in Figure 11, physical parameters for the feature are estimated to construct a polyhedron model. Initially, the feature is represented as a flattened cylindrical tube where the length and width of the shape model are inferred from the map signature. Then, the depth of the structure is estimated using the same width/depth ratio that is associated with Schroeter Vallis. As apparent in Figure 11, the signature is not linear but sinuous; to reflect this aspect, the initial linear profile, that is, the cylinder, is morphed to a curve that represents the approximate center line for the map signature. Physical parameters for the resulting shape model are summarized in Table 2 and the polyhedron shape model is illustrated in Figure 12(a). Also, represented in Figure 12(b) is the projection of the vertices of the polyhedron shape model onto the lunar surface, the center line profile that is employed to morph the initial linear shape model to a sinuous profile, and an estimated contour of the map anomaly in blue, red, and black, respectively. In addition, the local topography is overlaid in the background, characterized by an absence of significant surface features.

Table 2. Forward model for Rima Sharp anomaly

λ, deg	ϕ, deg	length, km	depth, km	width, km
314	36	75	0.6	2

Then, as discussed previously in Section III.D, the simulation is repeated incorporating the gravitational potential and the acceleration due to the shape model. Note that the density for the structure is equal to 2560 $kg.m^{-3}$ to be consistent with the Bouguer model, however, it is not consistent with the density of mare basalt, the material that constitutes most of the mare. The resulting averaged map with the forward model

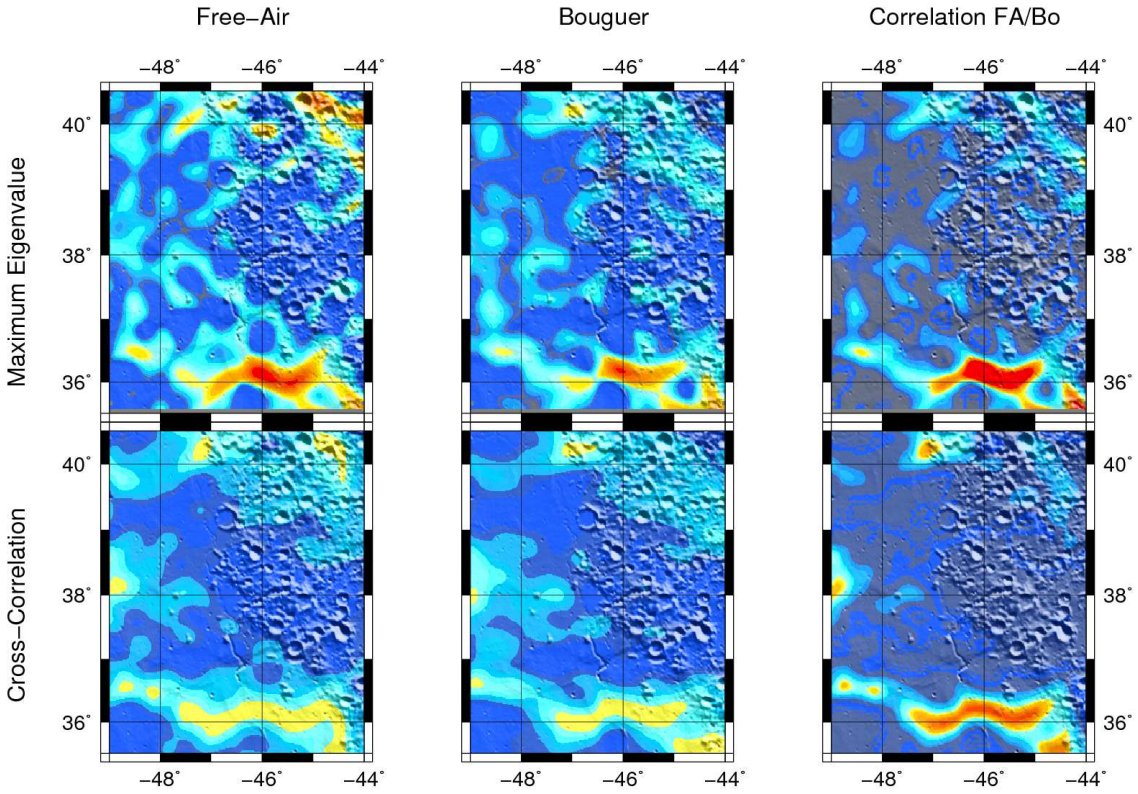

Figure 11. Local cross-correlation and eigenvalue map in the Rima Sharp region with overlay of the topography.

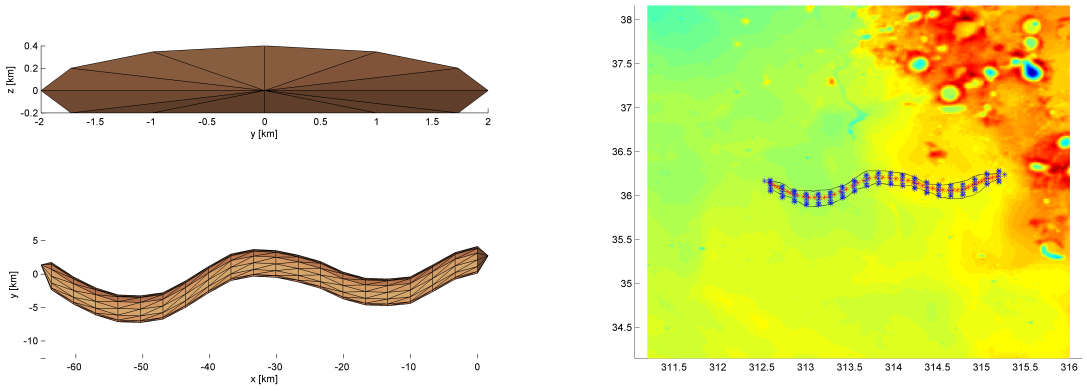

(a) Shape model

(b) Footprint

Figure 12. Forward model for Rima Sharp anomaly

appears in Figure 13. In the figure, the top row corresponds to the gradiometry and cross-correlation map without the addition of the forward model, and the signature of interest appears in the south center of each map. The bottom row of plots illustrates the result of incorporating the forward model in the simulation. Similar to the Schroeter analysis, the gradiometry map that includes the forward model does not exhibit the initial anomaly signature, that is, the forward model is successful in matching the gravity anomaly that is observed on the initial gradiometry map. For the cross-correlation strategy, however, the forward model approach is not as successful, and further investigation is required to better characterize the feature and improve the performance of the cross-correlation analysis within this context. Also, note that these maps are preliminary results and the product of a simulation with a forward model that is constructed based on one set of parameters. Since gravity is non-unique, an infinite number of solutions can fit a given gravity anomaly. The task then consists in identifying the set of parameters that yield the best fit with respect to the observed signature on the maps.

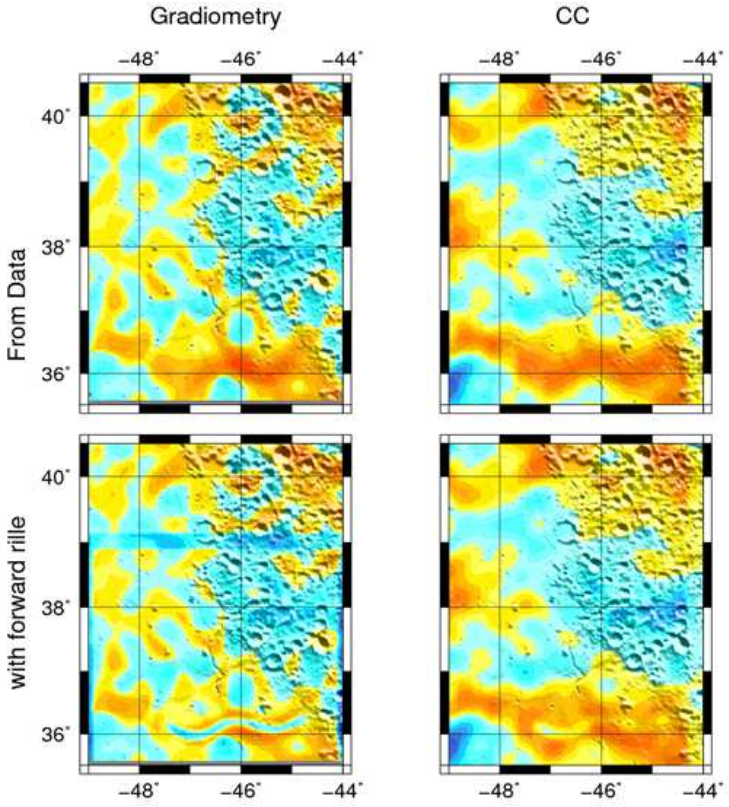

Figure 13. Local cross-correlation and eigenvalue map in the Rima Sharp region with forward model for observed anomaly.

VI. Toward a Global Search

To further extend the search for buried empty lava tubes, the detection strategy and validation tools based on gradiometry and cross-correlation analysis are employed towards covering the mare regions of the Moon. In 2012, Hurwitz, Head and Hiesinger characterized the distribution of sinuous rilles and developed a global map of such features over the lunar surface.[12] The majority of the 194 features observed with LROC WAC and SELENE LISM lie on the lunar nearside with a concentration in the mare region of the Moon. Sublunar voids and skylights have also been identified by Robinson in 2012.[8] Such developments and findings promote the ongoing search for uncollapsed lava tubes in the vast mare regions.

VI.A. Strategy

The analysis is focused on the lunar nearside, the region on the Moon that contains most known sinuous rilles. The lunar nearside is divided into two major regions of investigation, as illustrated in Figure 14. A first region, Region A, ranges from 0-60 degrees East and 0-60 degrees North. Similarly, a second region, Region B, extends from 300-360 degrees East and 0-60 degrees North. The red dot in the figure marks the relative location of Schroeter Vallis on the nearside of the Moon. For detailed analysis, an array of grids, similar to those in yellow, is created by dividing the blue region, already a subset of the larger red Region A, into 6 by 5 degree grids. Then, the two detection strategies, gradiometry analysis and cross-correlation, are employed on the array of grids to produce corresponding maps. Based on different models, applied truncations and tapers, an average map and a dynamic simulation are created. The animation layers numerous maps resulting from different models, truncations and tapers onto a topographical map of the area. This methodology aids in identifying signals that are persistent between different maps and differentiates them from numerical noise.

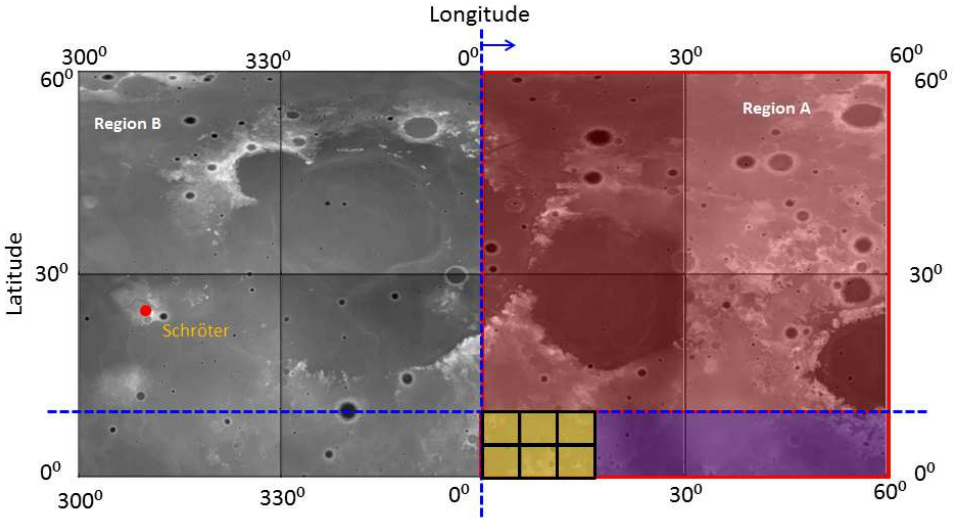

Figure 14. Nearside region under investigation.

VI.B. Vicinity of Schroeter Vallis

Gravitational anomalies observed at Schroeter Vallis motivate further investigation of the region that lies in the vicinity. Eight grids are collected in Figure 15, in cardinal and inter-cardinal directions relative to Schroeter Vallis, and this set is examined using the detection strategies. Localized free-air and Bouguer potential maps overlaid with topography are created using gradiometry and cross-correlation detection strategies for each individual grid. Figure 15 illustrates free-air potential maps based on local averaged eigenvalues with regional topography. The free-air analysis identifies gravitational anomalies due to surface features as well as buried structures. As previously noted, the color scale represents the magnitude of the largest eigenvalue of the Hessian derived from the gravitational potential. A resulting animation for each grid is visually inspected to recognize and validate signals that are persistent over different models, truncations and tapers. Additional gravitational anomalies noted from free-air representations that do not correspond to surface features, suggest some form of subsurface negative gravitational anomaly. Specifically, anomalies in the central, northeastern, eastern and southeastern grids appear that do not match the surface topography and are persistent throughout the visual analysis of the animation. Such negative gravity anomalies, or mass deficit, suggest the existence of buried structures, such as buried craters or potential lava tubes. The digit in each grid in Figure 16 represents the number of anomalies detected in a particular 6 by 5 degree grid. Each individual grid corresponds to the coverage over a spatial area of approximately 180 km by 150 km. The numeral in the central grid corresponds to the Schroeter Vallis anomaly. The adjacent grids suggest three additional gravitational anomalies in the vicinity of Schroeter Vallis denoted by a number 1. No additional features are clearly detected based on the algorithm in the remaining adjacent grids as denoted by the number 0. The search methodology provides a structural framework that aids in recognizing the features.

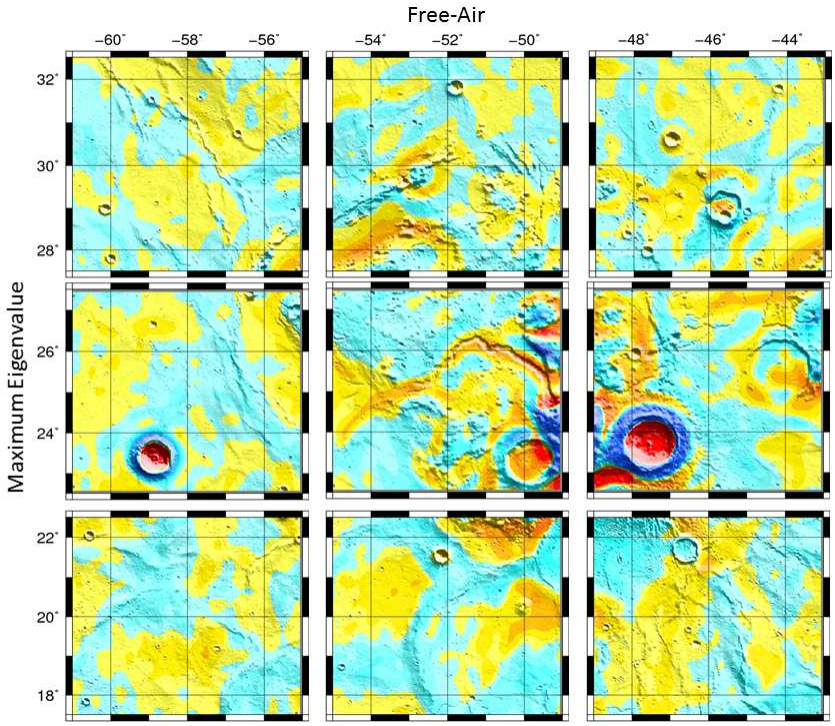

Figure 15. Free-air averaged eigenvalue map for Schroeter Vallis and its vicinity.

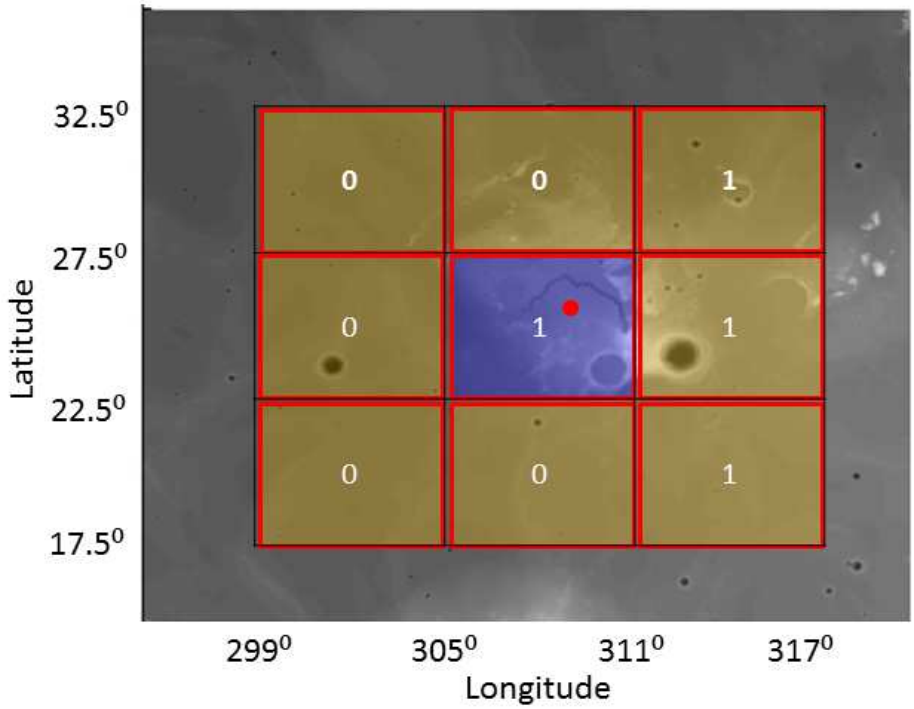

Figure 16. Region in the vicinity of Schroeter Vallis.

VII. Conclusion

The success of the NASA's GRAIL mission ensures that the highest resolution and most accurate gravity data for the Moon is now available. The low altitude at which some of these data were collected in the GRAIL extended mission potentially allows the detection of small-scale surface or subsurface features. The focus of this analysis is the specific task of detecting the potential presence and extent of empty lava tubes beneath the mare surface. In this investigation, tools are developed to best exploit the rich gravity data and advance the numerical detection of these small features. Two independent strategies are considered: one based on gradiometry techniques and a second that relies on cross-correlation of individual tracks. Both approaches are combined into an automated algorithm that aims to construct local maps of the lunar surface and highlight the possible detection of the features of interest. In addition, forward modeling is leveraged to further validate possible detections and to attempt to characterize the physical parameters of a feature. The proposed algorithm is first validated using Schroeter Vallis, the largest known lunar sinuous rille, as a test feature. This rille is successfully detected with both strategies and this simulation offers a first validation of the tool. Forward modeling applied to this scenario also demonstrates the ability to represent the feature of interest with a simple model to further support the detection and initially characterize the structure that is identified.

Some limitations and challenges remain. The size of the structures that are the object of this analysis is near the same order of magnitude or smaller than the resolution of the gravity data. It is then challenging to determine whether an observed signal on an eigenvalue or cross-correlation map is, in fact, the signature of a physical structure or is a numerical artifact. Also, numerical challenges are associated with spherical harmonics analysis for very high degree and order. To assess the robustness of an observed signal, rather than considering a single simulation, numerous computations are considered to produce an averaged map. A second test is also incorporated that aims to demonstrate some success, despite these challenges, the proposed algorithm is able to alleviate the numerical effects and produce maps that do not produce any significant signatures in a region that does not exhibit noteworthy features. Then, another region near a South channel of Rima Sharp is introduced, where a persistent anomaly consistent with an underground mass deficit is identified. The anomaly is observed on both Bouguer and free-air maps that are produced with both strategies, gradiometry and cross-correlation, thus, strongly suggesting the presence of an underground mass deficit that corresponds to the gravity anomaly that is apparent.

Finally, in an initial step toward inspecting the entire mare region on the Moon, a global search strategy is introduced. In addition to extending the analysis to completely inspect the lunar mare, continuing work includes exploiting KBRR track data directly. Also, forward modeling to characterize the signatures observed on the maps requires further investigation.

References

[1]Zuber, M., Smith, D., Lehman, D., Hoffman, T., Asmar, S., and Watkins, M., "Gravity Recovery and Interior Laboratory (GRAIL): Mapping the Lunar Interior from Crust to Core," *Space Science Reviews*, Vol. 178, No. 1, 2013, pp. 3–24.

[2]Tapley, B. D., Bettadpur, S., Ries, J. C., Thompson, P. F., and Watkins, M. M., "GRACE Measurements of Mass Variability in the Earth System," *Science*, Vol. 305, No. 5683, 2004, pp. 503–505.

[3]Zuber, M. T., Smith, D. E., Watkins, M. M., Asmar, S. W., Konopliv, A. S., Lemoine, F. G., Melosh, H. J., Neumann, G. A., Phillips, R. J., Solomon, S. C., Wieczorek, M. A., Williams, J. G., Goossens, S. J., Kruizinga, G., Mazarico, E., Park, R. S., and Yuan, D.-N., "Gravity Field of the Moon from the Gravity Recovery and Interior Laboratory (GRAIL) Mission," *Science*, Vol. 339, No. 6120, 2013, pp. 668–671.

[4]Konopliv, A. S., Park, R. S., Yuan, D.-N., Asmar, S. W., Watkins, M. M., Williams, J. G., Fahnestock, E., Kruizinga, G., Paik, M., Strekalov, D., Harvey, N., Smith, D. E., and Zuber, M. T., "High-resolution lunar gravity fields from the GRAIL Primary and Extended Missions," *Geophysical Research Letters*, Vol. 41, No. 5, 2014, pp. 1452–1458.

[5]Lemoine, F. G., Goossens, S., Sabaka, T. J., Nicholas, J. B., Mazarico, E., Rowlands, D. D., Loomis, B. D., Chinn, D. S., Neumann, G. A., Smith, D. E., and Zuber, M. T., "GRGM900C: A degree 900 lunar gravity model from GRAIL primary and extended mission data," *Geophysical Research Letters*, Vol. 41, No. 10, 2014, pp. 3382–3389.

[6]Angelis, D. G., Wilson, J., Clowdsley, M., Nealy, J., Humes, D., and Clem, J., "Lunar Lava Tube Radiation Safety Analysis," *Journal of Radiation Research*, Vol. 43, No. Suppl, 2002, pp. S41–S45.

[7]Haruyama, J., Hioki, K., Shirao, M., Morota, T., Hiesinger, H., van der Bogert, C. H., Miyamoto, H., Iwasaki, A., Yokota, Y., Ohtake, M., Matsunaga, T., Hara, S., Nakanotani, S., and Pieters, C. M., "Possible lunar lava tube skylight observed by SELENE cameras," *Geophysical Research Letters*, Vol. 36, No. 21, 2009.

[8]Robinson, M., Ashley, J., Boyd, A., Wagner, R., Speyerer, E., Hawke, B. R., Hiesinger, H., and van der Bogert, C., "Confirmation of sublunarean voids and thin layering in mare deposits," *Planetary and Space Science*, Vol. 69, No. 1, 2012, pp. 18 – 27.

[9]Butler, D. K., "Microgravimetric and gravity gradient techniques for detection of subsurface cavities," *Geophysics*, Vol. 49, No. 7, 1984, pp. 1084–1096.

[10]Sharpton, V. L., Grieve, R. A. F., Thomas, M. D., and Halpenny, J. F., "Horizontal gravity gradient: An aid to the definition of crustal structure in North America," *Geophysical Research Letters*, Vol. 14, No. 8, 1987, pp. 808–811.

[11]Cordell, Lindrith, 1979, Gravimetric expression of graben faulting in Santa Fe country and the Espanola Basin, New Mexico, in: Santa Fe Country, Ingersoll, Raymond V.; Woodward, Lee A.; James, H. L., New Mexico Geological Society, Guidebook, 30th Field Conference, pp. 59-64.

[12]Hurwitz, D. M., Head, J. W., and Hiesinger, H., "Lunar sinuous rilles: Distribution, characteristics, and implications for their origin," *Planetary and Space Science*, Vol. 7980, No. 0, 2013, pp. 1 – 38.

[13]Smith, D. E., Zuber, M. T., Jackson, G. B., Cavanaugh, J. F., Neumann, G. A., Riris, H., Sun, X., Zellar, R. S., Coltharp, C., Connelly, J., Katz, R. B., Kleyner, I., Liiva, P., Matuszeski, A., Mazarico, E. M., McGarry, J. F., Novo-Gradac, A.-M., Ott, M. N., Peters, C., Ramos-Izquierdo, L. A., Ramsey, L., Rowlands, D. D., Schmidt, S., Scott, V. S., Shaw, G. B., Smith, J. C., Swinski, J.-P., Torrence, M. H., Unger, G., Yu, A. W., and Zagwodzki, T. W., "The Lunar Orbiter Laser Altimeter Investigation on the Lunar Reconnaissance Orbiter Mission," *Space Science Reviews*, Vol. 150, Jan. 2010, pp. 209–241.

[14]Kiefer, W. S., Macke, R. J., Britt, D. T., Irving, A. J., and Consolmagno, G. J., "Regional Variability in the Density of Lunar Mare Basalts and Implications for Lunar Gravity Modeling," *Lunar and Planetary Science Conference*, Vol. 43 of *Lunar and Planetary Science Conference*, March 2012, p. 1642.

[15]Andrews-Hanna, J. C., Asmar, S. W., Head, J. W., Kiefer, W. S., Konopliv, A. S., Lemoine, F. G., Matsuyama, I., Mazarico, E., McGovern, P. J., Melosh, H. J., Neumann, G. A., Nimmo, F., Phillips, R. J., Smith, D. E., Solomon, S. C., Taylor, G. J., Wieczorek, M. A., Williams, J. G., and Zuber, M. T., "Ancient Igneous Intrusions and Early Expansion of the Moon Revealed by GRAIL Gravity Gradiometry," *Science*, Vol. 339, No. 6120, 2013, pp. 675–678.

[16]Werner, R. A., "The Gravitational Potential of a Homogeneous Polyhedron or don't Cut Corners," *Celestial Mechanics and Dynamical Astronomy*, Vol. 59, No. 3, 1993, pp. 253–258.

[17]Chappaz, L., "The Dynamical Environment in the Vicinity of Small Irregularly-Shaped Bodies and Application to Asteroids," M.S. Thesis, School of Aeronautics and Astronautics, Purdue University, West Lafayette, Indiana, December 2011.

[18]Chappaz, L. and Howell, K., "Bounded Orbits near Binary Systems Comprised of Small Irregular Bodies," *AIAA/AAS Astrodynamics Specialist Conference*, San Diego, California, August 2014.